Quantum Electronics **49** (2) 199–204 (2019)

https://doi.org/10.1070/QEL16885

Optical frequency reference for the national time scale

D.V. Sutyrin, O.I. Berdasov, S.Yu. Antropov, A.Yu. Gribov, R.I. Balaev, E.F. Stel'mashenko, D.M. Fedorova, A.N. Malimon, S.N. Slyusarev

Abstract. **Incorporation of a strontium optical clock as an optical frequency reference into the primary standard GET 1-2018 is experimentally implemented. A new model is proposed to define a local atomic time scale using an optical reference incorporated into a complex for reproducing primary standard units. Preliminary results of comparing the frequencies of the optical reference and the hydrogen maser entering the composition of primary time and frequency standards are presented.**

Keywords: *optical frequency standard, strontium atoms, primary standard, national time scale.*

1. Introduction

Time and frequency – physical quantities that can be measured with least uncertainty – play a particular role in physics. Atomic frequency standards based on the reference transition between the energy levels of the ^{133}Cs ground level hyperfine structure define the second in the International System of Units (SI). The relative frequency uncertainty for the best cesium fountains is at the level of few units of 10^{-16} [1, 2]. However, optical frequency standards (OFS's) demonstrate better frequency stability and accuracy. OFS's based on different atoms and reference transitions have already been developed [3–11] or are being actively developed in leading metrological centres and scientific laboratories of the world. The research in this field is motivated by the necessity of redefining the second in SI based on a quantum transition in the optical range [12] or reducing the local time scale uncertainty.

The OFS's based on cold atoms in an optical lattice showed a systematic frequency uncertainty at the level of 10^{-17}–10^{-18} [7] and a better frequency stability [13]. Due to this, the OFS frequencies can be compared with a smaller error and for a shorter time than in the case of microwave references [14]. In particular, several research teams developed OFS's based on neutral strontium atoms [15–17].

An OFS based on neutral ^{87}Sr atoms was developed at the Russian Metrological Institute of Technical Physics and Radio Engineering (VNIIFTRI). This OFS was incorporated into the complex for reproducing time and frequency units of the primary standard GET 1-2018. In this paper, we propose a new mathematical model of time scale formation, in which an OFS is considered as one of frequency references, on a par with caesium and rubidium fountains; i.e., it plays the role of an optical frequency reference (OFR). This is consistent with the officially accepted model for forming the Coordinated Universal Time UTC(SU) scale at the level of 3×10^{-16} for an observation time of 7 months. Experimental implementation of regular comparisons of OFR frequencies with the frequencies of other references within the new model is performed during data accumulation on a long time interval.

2. Motivation of the study

Impressive progress in the OFS formation [13, 18–25] has provoked discussion about the necessity of redefining the SI second [12, 23, 24]. The first step in this direction was the detection of appropriate optical transitions in order to perform a secondary second redefinition by the International Bureau of Weights and Measures [25, 26]. Currently, the question of practical realisability of redefinition of the SI second is being actively investigated at the leading metrological centres of the world [17, 27, 28]. The problem is that, generally speaking, OFS's do not operate continuously, a circumstance important for practical time scale (TS) implementation.

To date, the UTC is formed by post-processing the monthly weighted mean of time, which is stored by 500 microwave atomic clocks of national primary standards of the world. Practical applications call for free access to the time value at any instant. Therefore, each national primary standard generates its own local TS in real time, which is bound to the frequency of a continuously operating microwave generator, for example a hydrogen maser (HM). This approach makes it possible to synchronise a local TS with the UTC scale during a month. The metrological centres at which primary references are located synchronise their HMs on a shorter time interval by comparing their frequencies with the frequencies of caesium references.

Due to the averaging, the UTC scale is more stable than that of most local TS's, whose accuracy is limited by the accuracy of atomic reference and its rest periods. Thus, in practice, the quality of a local TS is generally estimated by comparing it with the UTC scale. However, the UTC scale is not an ideal

D.V. Sutyrin, S.Yu. Antropov, R.I. Balaev, E.F. Stel'mashenko, A.N. Malimon, S.N. Slyusarev Russian Metrological Institute of Technical Physics and Radio Engineering, 141570 Mendeleevo, Moscow region, Russia; e-mail: sutyrin@vniiftri.ru, amalimon@mail.ru, serslyu@mail.ru, santro@mail.ru;
O.I. Berdasov, A.Yu. Gribov, D.M. Fedorova Russian Metrological Institute of Technical Physics and Radio Engineering, 141570 Mendeleevo, Moscow region, Russia; National Research Nuclear University 'MEPhI', Kashirskoe sh. 31, 115409 Moscow, Russia; e-mail: berd_7@mail.ru, gribov.art@mail.ru, dmfedorova@vniiftri.ru

Received 24 October 2018; revision received 23 November 2018
Kvantovaya Elektronika **49** (2) 199–204 (2019)
Translated by Yu.P. Sin'kov

reference, and the difference between it and the TS generated by a local caesium reference may reach 0.1 ns per day.

The time error of local TS's can be decreased by more than an order of magnitude using OFRs [17]; this decrease should improve their predictability. The development of an optical clock network with simultaneous improvement of time transfer technology [29] will make it possible to design much more stable TS's than the UTC scale. This is extremely important for global navigation systems, astrophysics, and fundamental science.

3. OFR as an element of the complex for reproducing time and frequency units

3.1. Relationship between OFR and classical frequency references

The complex for reproducing time and frequency units of the State primary standard of time and frequency units and the national time scale (GET 1-2018) contains two metrological caesium standards (MCS's) and an OFR based on cold strontium atoms. The confidence limits of the non-excluded systematic error in reproducing frequency units by the primary reference do not exceed 5×10^{-16} at the confidence probability level of 0.99.

A complex for storing the national TS also enters the GET 1-2018 composition. This complex contains a set of HMs, which play the role of keepers of frequency and time units, with a long-term frequency instability smaller than 5×10^{-16} on the measurement time interval of 24 h. Along with the HMs, this complex contains also keepers based on a rubidium atomic fountain [30]. Note that the MCS and OFR are switched on periodically, while the HMs work continuously, thus storing the units and TS. The frequency generated by each HM is determined by comparing it with the reference frequency.

The OFR is installed in an optical laboratory, located at a distance of about 1 km from the building containing the set of HMs and microwave references entering the GET 1-2018 composition. There is also a base HM 18 in the same laboratory; the OFR frequency is measured with respect to the frequency of this maser. To determine the OFR absolute frequency, the frequency of the base HM 18 should be compared with that of the HM keepers entering the GET 1-2018 composition. To carry out these comparisons, the output signal of HM 18 with a frequency of 5 MHz is transferred by an optical carrier with a wavelength of 1.3 μm via a fibre cable to the phase comparators of the GET1-2018 complex for keeping the national TS. To increase the comparison reliability, the 10-MHz output signal of HM 44 (one of the GET 1-2018 keepers) is transferred via a fibre cable to the optical laboratory. The HM 44 and HM 18 frequencies are compared using a comparator mounted in the optical laboratory. Tests showed that the frequency instability introduced additionally by the system of transferring standard signals through a fibre cable does not exceed 2×10^{-16} on the measurement time interval of 24 days.

Figure 1 shows typical results of comparing the HM frequencies measured at the OFR Laboratory and at the Primary Time and Frequency Standard (PTFS) Exploitation Department. The rise of the curve for the comparisons between HM 18 and HM 44 on averaging ranges of 100–1000 s is explained by the periodicity of switching on a conditioner located in the room with measuring equipment.

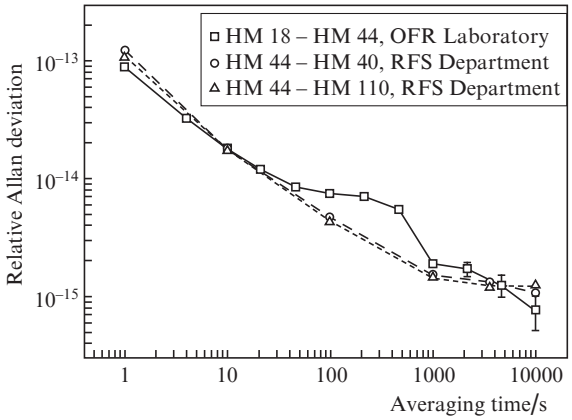

Figure 1. Result of comparing the HM frequencies at the OFR Laboratory and at the PTFS Exploitation Department [RFS (Reference Frequency Standard) Department]. Squares are the results of comparing the HM 18 and HM 44 frequencies using a comparator located at the OFS Laboratory. Circles and triangles are the results of comparing the HM 44 frequencies with the HM 40 and HM 110 frequencies using a comparator installed at the PTFS Department. The rise of the comparison curve for HM 18 and HM 44 on the averaging ranges of 100–1000 s is explained by the periodicity of switching on the air conditioner in the room with measuring equipment.

Furthermore, it is planned to eliminate the effect of the temperature instability due to these switchings by placing the comparison equipment in a special box with constant climatic conditions.

3.2. OFR based on strontium atoms

The structure and principles of operation of the OFR based on ^{87}Sr atoms were described in detail in [31–33]. The main OFR components are an atomic spectroscope, laser systems for cooling and capturing atoms into an optical trap, a laser system with an external high-finesse ultra-low expansion (ULE) cavity for spectroscopy of the $^1S_0 - {}^3P_0$ 'clock' transition in ^{87}Sr atoms, and a system for controlling OFR operation cycles. To compensate for the change in the 'clock' laser frequency caused by the ULE cavity drift, an acousto-optic modulator is used to tune the laser frequency to the atomic transition resonance. The tuning frequency is calculated in each operation cycle based on the 'clock' transition spectroscopy data. The currently used scheme for comparing OFR with primary standard is presented in Fig. 2.

In contrast to the scheme used in [31], HM 18 and OFR are installed in the same room. To transfer the OFR characteristics to the RF range, part of the laser radiation tuned to the clock transition frequency is used to stabilise the optical beat frequency f_{beat} between the laser frequency and the corresponding mode of femtosecond optical synthesiser (FOS). The FOS mode frequency is $\nu_m = f_{ceo} + mf_{rep}$, where f_{ceo} is the carrier–envelope offset frequency, f_{rep} is the pulse repetition frequency in the FOS cavity, and m is an integer (FOS mode number). In our case, a commercial fibre synthesiser with frequencies $f_{rep} \approx 250$ MHz and $f_{ceo} = 20$ MHz (the latter is stabilised with respect to HM 18) is used as an FOS. The FOS signal with a frequency f_{rep} is recorded by a fast photodetector and mixed in an RF mixer with a signal from a commercial RF synthesiser (~240 MHz), to which a reference 10-MHz signal from HM 18 is supplied. The difference signal from the mixer is supplied to one of the dead-time-free K + K FXE

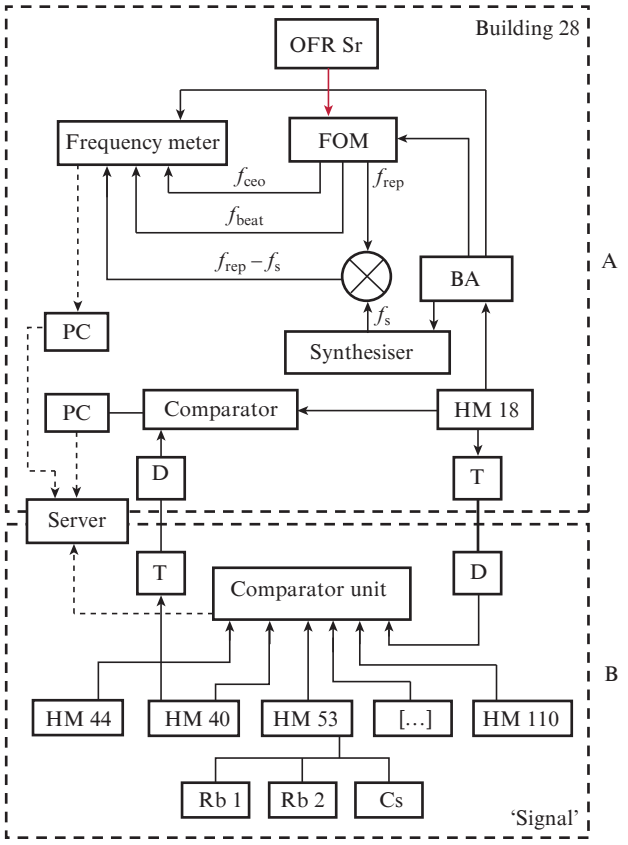

Figure 2. Comparison scheme: (BA) buffer amplifier for distributing the 10-MHz signal; (T) optical transmitter of a signal with a frequency of 5/10 MHz; (D) optical detector of the 5/10-MHz signal; (PC) personal computer; (Synthesiser) RF synthesiser with $f_s \approx 240$ MHz; (FOS) femtosecond optical synthesiser of frequencies $f_{ceo} = 20$ MHz, $f_{beat} = 60$ MHz, and $f_{rep} \approx 250$ MHz; (Rb 1, Rb 2) rubidium fountains; (Cs) caesium fountain; (HM 18, 44, 40, 53, 110) hydrogen masers that are key for measurements; ([…]) other hydrogen masers. Rectangles A and B denote separate buildings, spaced at a distance of about 1 km.

counters of the frequency meter. The measurement data from the frequency meter are transferred via a local network for computer processing. The absolute OFR frequency is determined with respect to the HM 18 frequency as $\nu_{Sr} = f_{ceo} + mf_{rep} + f_{beat}$, where m is the number of the FOS mode nearest to the clock laser frequency.

Gravitational frequency shift. To determine the gravitational shift for the OFR, we measured its location altitude in the Baltic system of heights and the acceleration of gravity at the sample location point. The height was measured by a digital level DNA03 to be 212.0091 m with an rms excess measurement error of 28 cm. The local acceleration of gravity was determined by a SCINTREX CG-5 AUTOGRAV gravimeter with a relative measurement error of 5×10^{-8} m s^{-1}. The acceleration of gravity was found to be 9.8157 m s^{-2}, and the relative frequency shift under these conditions was $\delta_G = -2.32 \times 10^{-14} \pm 7 \times 10^{-17}$.

Frequency shift due to the black body radiation. The most significant frequency shift in an OFR is the Stark shift Δf_{BBR}, which is caused by the thermal radiation from the environment. At room temperature

$$\Delta f_{BBR} = -0.5(\alpha^{(0)}_{3P0} - \alpha^{(0)}_{1S0})\langle E^2(T)\rangle\,[1 + \eta(T^2)]. \qquad (1)$$

To determine this shift, one must know exact values of the differential static polarisabilities of the ground and excited states of the clock transition α (for Sr atoms $\alpha_{1S0} = 197.2(2)$, $\alpha_{3P0} = 458.3(3.6)$ [34]), the dynamic correction parameter η, and the averaged field emitted by an absolutely black body at a temperature T. The theoretical calculation performed in [35] makes it possible to pass from (1) to the expression

$$\Delta f_{BBR} = -2.13023\left(\frac{T}{300\text{K}}\right)^4 - 0.1476\left(\frac{T}{300\text{K}}\right)^6. \qquad (2)$$

The chamber temperature, stabilised due to the water cooling of magnetic coils and maintaining the room temperature at a level of about 21 °C, was measured by a fixed sensor to be 20 ± 1 °C. After substituting the found temperature value into expression (2), we obtain the following value for the relative frequency shift due to thermal radiation: $\Delta f_{BBR}/f \approx -4.66 \times 10^{-15} \pm 6.99 \times 10^{-17}$.

Stark frequency shift caused by the laser radiation forming an optical lattice. The frequency of the laser radiation forming an optical lattice at the 'magic' wavelength of 813.427270 nm [35] was stabilised in our case using an Angstrom WS U2 wavelength meter and maintained with an error of 2 MHz. The laser power is 500 mW, and the lattice depth is determined from the side band frequency, which was found from 1-h spectroscopic measurement to be ~53430 Hz. The error in measuring the frequency shift is determined by the wavelength meter measurement error; for the lattice-forming laser stabilised with respect to the meter, this error is 2.53×10^{-17}.

3.3. Mathematical model of atomic time formation

To determine the characteristics of the developed OFR, it was incorporated into the system for comparing the frequencies of the HM set and ^{133}Cs and ^{87}Rb microwave frequency references, entering the composition of GET 1-2018 (Fig. 3). The operation of the microwave references and OFR is not continuous. The frequencies of the microwave references and OFR were collated by comparing their frequencies with those of constantly operating HMs.

For 7 months, since March 1, 2018, a specialised software fixed mutual deviations of HM frequencies in the form of arrays $\delta f_{ij}(t)$ of daily average values of pair frequency differences for generators i and j. The frequency deviations for the base HMs (connected to the frequency reference), observed during frequency reference operation sessions, were fixed in the form of pair frequency differences $\delta f_{rb}(t)$ for the reference (r) and base (b) HMs, reduced to 12:00 am.

The frequency unit is transferred (by software means) from the references (Rb, Cs) to HM every day, according to the observation data for a period beginning from 3 to 5 months before the transfer onset; it ceases when the last frequency comparison session for the base HM and reference is finished. The data from the arrays of each pair frequency difference $\delta f_{ij}(t)$ are approximated by a second-order polynomial using the least-squares method. The linear model $M[i-j](t) = a_{ij} + b_{ij}t$, which predicts the frequency difference drift for generators i and j, as well as for the base generator and frequency reference, $M[\text{b} - \text{r}](t) = a_{br} + b_{br}t$, is defined as the equation of the tangent to this polynomial at the point corresponding to the end of approximation interval (Fig. 4).

A concept of atomic system frequency f_A is introduced for the system of HM and frequency references shown in Fig. 3.

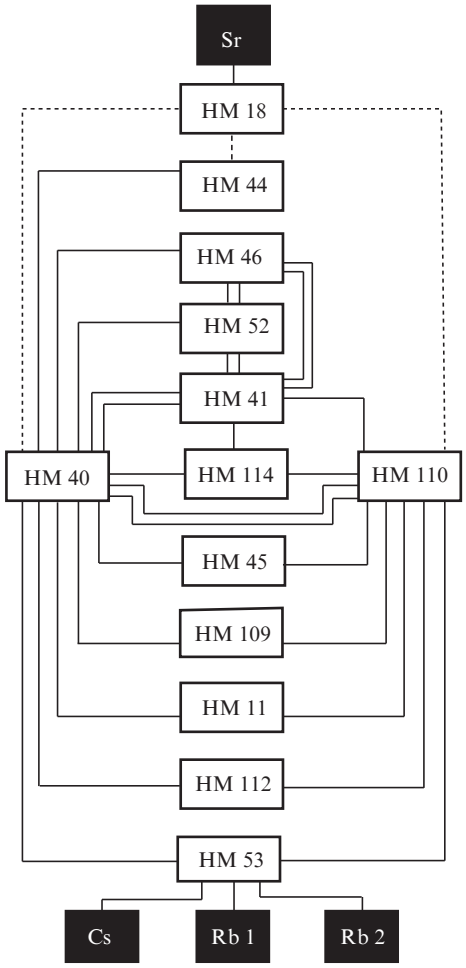

Figure 3. Generator frequency intercomparison scheme. Solid lines are observation channels of the intercomparison system, which fix time dependences of pair frequency differences, and dotted lines are optical communication channels ~1 km long.

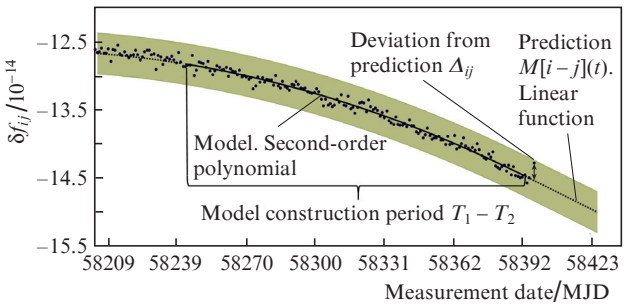

Figure 4. Results of measuring pair frequency differences (dots), approximation by a second-order polynomial on the $T_1 - T_2$ time interval (solid line), and a linear prediction corresponding to the polynomial tangent at the point T_2 (dotted line).

The $\delta f_{i\mathrm{A}}$ value is calculated by the software as a set of corrections to the frequencies of individual HMs, $\delta f_{i\mathrm{A}}$, which are determined for the instant t_0 as

$$\delta f_{i\mathrm{A}}(t_0) = M[i - \mathrm{A}](t_0) + \Delta_{i\mathrm{A}}(t_0), \tag{3}$$

where $M[i - \mathrm{A}](t_0)$ is the deviation of the ith-HM frequency from the atomic system frequency, predicted based on previous observations, and $\Delta_{i\mathrm{A}}(t_0)$ is the deviation of the ith-HM frequency from the predicted value, $M[i - \mathrm{A}](t_0)$, estimated from the pair frequency differences $\delta f_{ij}(t_0)$ observed at the instant t_0.

The model predicting the frequency drift for the ith HM with respect to the frequency reproduced by the atomic clock standard,

$$M[i - \mathrm{A}](t) = a_i + b_i t, \tag{4}$$

is determined by the system of equations

$$a_{ij} + b_{ij} t = a_i + b_i t - a_j - b_j t, \tag{5a}$$

$$a_{\mathrm{br}} + b_{\mathrm{br}} t = a_{\mathrm{b}} + b_{\mathrm{b}} t - \delta f_{\mathrm{rA}}, \tag{5b}$$

where δf_{rA} is the reference (r) frequency deviation from the frequency reproduced by the set of frequency standards of the atomic system. The number of equations in (5a) corresponds to the number of ij pairs (lines between white rectangles in Fig. 3). The number of equations in (5b) corresponds to the number of links originating from the frequency references (black rectangles in Fig. 3).

System of equations (5a) and (5b) is split into two subsystems with respect to the variables a_i and b_i; each of these subsystems is solved by the least-squares method. The thus found coefficients a_i and b_i determine the equation predicting the frequency drift for the ith standard relative to the value reproduced by the set of atomic system frequency standards (4).

The deviation of the ith-HM frequency from the predicted value $\Delta_{i\mathrm{A}}(t_0)$ is estimated based on the HM pair frequency differences $\delta f_{ij}(t_0)$ observed at the instant t_0 by solving the system of equations

$$\Delta_{ij}(t_0) = \Delta_{i\mathrm{A}}(t_0) - \Delta_{j\mathrm{A}}(t_0), \tag{6a}$$

$$0 = \sum_{i=1}^{n} \Delta_{i\mathrm{A}}(t_0), \tag{6b}$$

where $\Delta_{ij}(t_0) = \delta f_{ij}(t_0) - M[i - j](t_0)$ is the deviation of the observed pair frequency difference for the ith and jth generators from the predicted value. The number of equations in (6a) corresponds to the number of ij pairs (lines between white rectangles in Fig. 3); (6b) is the normalisation equation.

The set of equations (5), corresponding to the observation channels of the system of HM intercomparisons, describes all the links existing between the HMs. In fact, the normalisation equation (6b) sets the principle of fast estimation of the frequency deviation from model (4) for some HM. The sum of deviations from the model should be zero: it is assumed that the frequency deviation for the entire HM set is on average zero, i.e., corresponds to the average model.

Figure 5 shows the results of calculating the corrections $\delta f_{i\mathrm{A}}$ for the HM 110 during August 2018 and the official deviations of the frequency of this generator from the atomic time scale TA(SU), published in the Bulletin E [36]. The average difference of the values presented in Fig. 5 for the period from March 1, 2018, to October 8, 2018, is 3.3×10^{-16}; thus, the difference in the frequencies of the atomic system determined by the presented algorithm and the atomic system implemented in GET 1-2018 is within several units in the 16th decimal place.

The difference in the results is determined primarily by the application of only two rubidium frequency references; the

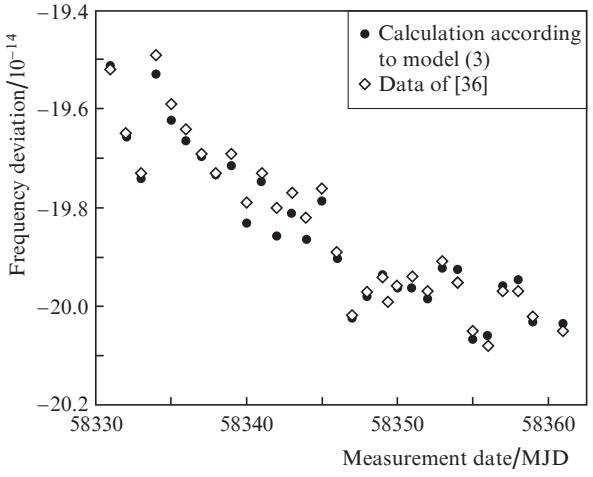

Figure 5. Deviation of the HM 110 frequency from the atomic system frequency, calculated according to formula (3), and the PTFS official data published in [36].

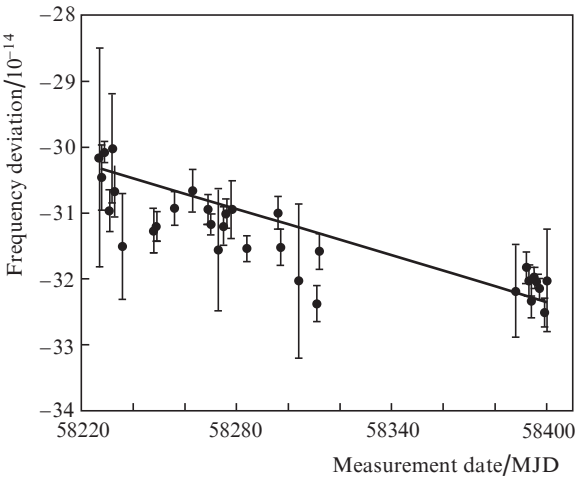

Figure 6. Experimental data on OFR and HM 18 frequency comparisons. Solid line is the result of calculation of HM 18 frequency drift from formula (4).

observation (intercomparison) scheme in use, which includes, in particular, an HM 18 generator connected with the tested optical frequency reference; and, finally, the algorithm for calculating δf_{iA}, which implies simultaneous use of all links (observation channels) between the HMs for frequency unit transfer, by solving system of equations (5) and (6) with application of the least-squares method.

4. Current results

As was mentioned in Section 2, an OFR cannot provide guaranteed continuous operation on diurnal range during several months. However, a quite appropriate regime is 10^4-s OFR operation several times a week for controlling the frequency of the HM involved in the formation of local TS [28]. Currently, we compare the frequency of strontium optical clock and the HM 18 frequency with this periodicity. Figure 6 shows the frequency drift for the HM 18, calculated according to model from Subsection 2.3, and the experimental results of comparison of OFR and HM 18 frequencies for a separate day and night. To date, measurements within the current comparison scheme were performed on the 58227–58399 MJD time interval (modified Julian date MJD = JD − 2400000.5, where JD is the Julian date; e.g., MJD = 58227 corresponds to 00:00, April 19, 2018). The first measurements on the 58220 − 58234 MJD interval are characterised by large errors caused by the tuning of the combined parts of the system. After a series of measurements (from 58313 to 58387 MJD), a pause was made to improve separate units of the system in order to increase the measurement period. A new series of measurements, which started at 58388 MJD, was characterised by a smaller spread of results. The rms value of the deviations of the HM 18 frequency from the OFR frequency, obtained in the sessions of the last series (7 sessions in total), turned out to be 1.6×10^{-15}. The Allan deviations of the differences between the HM 18 and atomic system frequencies, calculated according to (3) for averaging times of 24 and 72 h, are, respectively, 6×10^{-16} and 4×10^{-16}. Thus, when comparing the OFR and GET 1-2018 frequencies, the main sources of uncertainty arise during the comparison of the optical transition and HM 18 frequencies. The contribution of this component can be reduced by accumulating statistical data over many measurement sessions.

The presented experimental results are preliminary, because the number of measurements performed by the date of paper publication is insufficient for plotting the HM frequency drift with respect to the OFR and comparing it with the HM 18 drift, calculated according to the model described in Subsection 2.3. However, the stability and reliability of the system operation were significantly improved in the last series of measurements, and the error in comparing the OFR and HM 18 frequencies was essentially reduced; it is now determined by the instability of ambient temperature, which is planned to be diminished by locating a part of the measuring equipment in a chamber with constant climatic conditions.

5. Conclusions

A version of an experimental scheme for comparing an OFR with a set of hydrogen masers (frequency keepers) and caesium and rubidium standards was developed. A new algorithm was proposed for determining the frequency of the atomic system into which the OFR can be incorporated. Experimental comparisons of the HM frequency drift model were performed according to the algorithm and via collating with the OFR.

Continuation of measurements during the next several months will make it possible to determine finally the absolute OFR frequency with respect to the Cs and Rb standards and/or relative to the TAI (International Atomic Time) time scale, which is related to the UTC time scale. As a result, the OFR can be incorporated as a standard into the above-described mathematical model for determining the atomic time, along with caesium and rubidium frequency standards.

References

1. Blinov I. Yu. et al. *Measur. Techniques*, **60**, 30 (2017).
2. Levi F. et al. *Metrologia*, **51**, 270 (2014).
3. Poli N. et al. *Nuovo Cimento Rivista*, **36**, 555 (2013).
4. Pizzocaro M. et al. *Metrologia*, **54**, 102 (2017).

5. Huang Y. et al. *Phys. Rev. Lett*., **116**, 013001 (2016).
6. Huntemann N. et al. *Phys. Rev. Lett*., **116**, 063001 (2016).
7. Ushijima I. et al. *Nature Photon*., **9**, 185 (2015).
8. Yamanaka K. et al. *Phys. Rev. Lett*., **114**, 230801 (2015).
9. Lemke N D. et al. *Phys. Rev. Lett*., **103**, 063001 (2009).
10. Madej A. A. et al. *Phys. Rev. Lett*., **109**, 203002 (2012).
11. Rosenband T. et al. *Science*, **319**, 1808 (2008).
12. Gill P. *J. Phys.: Conf. Ser*., **723**, 012053 (2016).
13. Hinkley N. et al. *Science*, **341**, 1215 (2013).
14. Nemitz N. et al. *Nature Photon*., **10**, 258 (2016).
15. Hachisu H. et al. *Appl. Phys. B*, **123** (1), 34 (2017).
16. Lodewyck J. et al. *Metrologia*, **53**, 1123 (2016).
17. Grebing C. et al. *Optica*, **3** (6), 563 (2016).
18. Chou C.W. et al. *Phys. Rev. Lett*., **104**, 070802 (2010).
19. Dubé P. et al. *Phys. Rev. A*, **87**, 023806 (2013).
20. Bloom B.J. et al. *Nature,* **506**, 71 (2014).
21. Huntemann N. et al. *Phys. Rev. Lett*., **113**, 210802 (2014).
22. Godunet R.M. et al. *Phys. Rev. Lett*., **113**, 210801 (2014).
23. Riehle F.C.R. *Comptes Rendus*, **16** (5), 506 (2015).
24. Margolis H. *Nature Phys*., **10**, 82 (2014).
25. Riehle F. et al. *Metrologia*, **55**, 188 (2018).
26. https://www.bipm.org/utils/en/pdf/CIPM/CIM2013-EN.pdf.
27. Hachisu H. et al. *Sci. Rep*., **8**, 4243 (2018).
28. Hachisu H. et al. *Opt. Express*, **25** (8), 8511 (2017).
29. Śliwczýnski Ł. et al. *Metrologia*, **50**, 133 (2013).
30. Blinov I. et al. *European Frequency and Time Forum (EFTF)* (IEEE, 2018) p. 257. DOI:10.1109/EFTE.2018.8409045.
31. Berdasov O.I. et al. *Quantum Electron*., **48** (5), 431 (2018) [*Kvantovaya Elektron*., **48** (5), 431 (2018)].
32. Berdasov O.I. et al. *Quantum Electron*., **48** (5), 400 (2017) [*Kvantovaya Elektron*., **48** (5), 400 (2017)].
33. Khabarova K.Yu. et al. *Quantum Electron*., **45** (2), 166 (2015) [*Kvantovaya Elektron*., **45** (2), 166 (2015)].
34. Middelmann T.S. et al. *Phys. Rev. Lett*., **109**, 263004 (2012).
35. Westergaard P.G. et al. *Phys. Rev. Lett*., **106** (21), 210801 (2011).
36. ftp://ftp.vniiftri.ru/BULLETINS/E.